Article

Study on the Preparation of Cr-based Catalysts Doped by Zn using Sol–Gel Auto-Combustion Method and Its Application for Synthesis of 1-Chloro-2,3,3,4,4,5,5-heptafluorocyclopentene

Yajun Han,[a] Jinwei He,[a] Zhenhai Wu[a] and Xiaomeng Zhou[b]*

[a]*College of Environmental Science and Engineering, Nankai University, Tianjin 300071, China*
[b]*Economics and Management College, Civil Aviation University of China, Tianjin, China*

High-surface-area chromium-based catalysts in the presence of a small amount of zinc were prepared via a sol–gel auto-combustion method using chromic nitrate, zinc nitrate, and citric acid. First, the auto-combustion behavior of the dried gel was investigated by derivative thermogravimetry and (DTG)-TG and infrared (IR) techniques. The results revealed that the dried gel exhibited self-propagating combustion properties. Second, the as-burnt powders were characterized by IR, X-ray diffraction (XRD), Brunauer–Emmett–Teller analysis (BET), and scanning electron microscopy (SEM). The findings showed that the gels were directly converted into CrZn-O nanoparticles with high surface area during the auto-combustion process. Third, the pre-fluorination Cr-Zn catalysts were characterized by XRD, BET, SEM, X-ray photoelectron spectroscopy (XPS), and Fourier transform (FT)-IR spectroscopy of pyridine adsorption techniques. It was found that the presence of zinc led to significant structural changes in the catalyst, the particle size was smaller, the surface area became larger, and more active sites appeared. Finally, the catalytic activities of the samples were tested for the fluorination of 1,2-dichlorohexafluorocyclopentene (1,2-F6) with anhydrous hydrogen fluoride. The obtained results indicated that the pre-fluorination activated Cr-Zn catalysts prepared by this sol–gel auto-combustion method exhibited high efficiency in the synthesis of cyclic hydrofluorocarbons.

Keywords: Catalytic fluorination; Sol–gel auto-combustion method; 1-Chloro-2,3,3,4,4,5,5-heptafluorocyclopentene; Chromium oxide; Zinc.

INTRODUCTION

Chlorofluorocarbons (CFCs), hydrochlorofluorocarbons (HCFCs), and hydrofluorocarbons (HFCs) were widely used as refrigerants, foaming agents, cleaning agents, and etching agents in the past few years. However, because of their ozone depletion potential (ODP) and high global warming potential (GWP), the use of these haloalkanes has been limited by the Montreal Protocol and its subsequent amendments.[1–6] Recently, cyclic HFCs (c-HFCs), especially five-carbon rings, were identified as ideal alternatives to these because of their short atmospheric lifetimes, zero ODP, and low GWP.[7,8] However, due to the ring molecular structure and even unsaturated bonds, it is a serious challenge to achieve an efficient synthetic route for the c-HFCs.

Nowadays, the most common method to synthesize HFCs is vapor-phase catalytic fluorination of chlorinated hydrocarbons. However, the easily formed oligomers and cokes for c-HFCs make a more rigorous requirement for catalysts compared to HFCs. The currently known methods to produce c-HFCs commonly occur in the liquid phase, which is polluting and uneconomical. Thus, it is necessary for the industry to develop appropriate catalysts to produce c-HFCs by vapor-phase catalytic fluorination successfully.

For the fluorinated catalysts, the acid sites, surface area, particle size, and composition of the catalysts are important factors for their catalytic activity. Hence, nanoscale materials with high surface area and tunable surface properties have the potential to be used in c-HFCs synthesis.[9] Besides, chromium-based materials

---

*Corresponding author. Email: yajunhan110@163.com

are well-known catalysts for the F/Cl exchange reactions.[10–12] However, due to their high melting point, oxidation resistance, and poor sintering ability, nano-sized chromium materials are very difficult to prepare, and only a few patents have been reported up to now.[13] So the search for low-cost, high-efficiency nano-chromium-based catalyst production methods is still going on.

To produce nanoscale catalysts, many approaches such as plasma fluorination,[14] the sol–gel technique,[15] hydrothermal method,[16] and micro-emulsion synthesis[17] have been discussed. Compared to these methods, sol–gel auto-combustion method has many advantages such as cheap precursors and a simple preparation route,[18,19] Many superfine metal oxide powders with superior surface and bulk properties have been prepared through this method in the materials science field.[20–24] Therefore, the preparation of nano-scale chromium-based fluorination catalyst through sol–gel auto-combustion method has great value for industrial applications.

In this work, we prepared high-surface-area chromium-based catalysts in the presence of a small amount of zinc via the sol–gel auto-combustion method using chromic nitrate, zinc nitrate, and citric acid. Then, the dried gels, the as-burnt powders, and the activated catalyst were characterized by thermogravimetry-differential thermal analysis (TG-DTA), infrared (IR) spectroscopy, X-ray diffraction (XRD), Brunauer–Emmett–Teller (BET) analysis, scanning electron microscopy (SEM), X-ray photoelectron spectroscopy (XPS), and Fourier transform infrared (FT-IR) spectroscopy, Finally, the catalytic performance of the prepared catalysts was evaluated through the fluorination of 1,2-dichlorohexafluorocyclopentene (1,2-F6) with anhydrous hydrogen fluoride.

RESULTS AND DISCUSSION

Auto-combustion behavior

Experimental observation showed that the dried gel exhibited self-propagating combustion behavior. The curves of thermal analysis (TG and DTG) were plotted to study the auto-catalytic combustion process of the nitrate–citrate gel.

From Figure 1, it can be seen that the whole pyrolysis process of the dried gel can be divided into three stages. The first stage of weight loss in the 50–160°C range corresponds to the removal of residual moisture. The second stage of weight loss occurred in
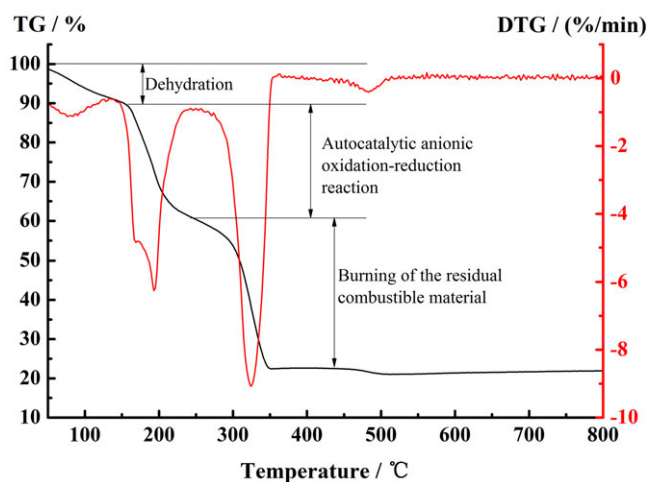

Fig. 1. TG and DTG thermograms of the dried citrate–nitrate gel CrZn(0) under air at the heating rate of 10°C/min.

the temperature range 160–250°C, which is attributable to the auto-catalytic anionic oxidation–reduction reaction between the nitrate and citrate. The decomposition of NH_4NO_3 produced by pH adjustment of the solution also took place in this temperature range. During the oxidation–reduction reaction, the nitrate ions provide an in situ oxidizing environment for the decomposition of the organic components,[25] lowering the decomposition temperature.[26] As expected, abundant amounts of gases such as CH_4, H_2, H_2O, and CO_2 were released. The peak of the DTG curve in the temperature range 160–250°C was relatively sharp, and the weight change associated with this reaction was ~25%. The final step in weight loss, which occurred between 250 and 500°C, signified the burning of the residual combustible material and decomposition of the carbonate complex to chromium oxide. There was a sharp peak in the DTG curve with a weight loss of ~40% in TG. As the temperature was further raised, there was no further weight loss and the DTG was zero. The weight loss for the entire process was ~77%. Notably, the thermal behavior of the other three gel precursors [CrZn(5), CrZn(15), and CrZn(25)] was basically the same as that of CrZn(0), which can be seen in Table 1. This is because the burning of the gels involved the nitrate and citrate ions but not the metal cation.

Characterization of gels and as-burnt powders

Figure 2 shows the IR spectra of the dried gels in the range 400–4000 cm^{-1}. The dried gel showed a

Table 1. TG of the CrZn(x) gels

Samples	Dehydration (°C)	Auto-catalytic anionic oxidation– reduction reaction (°C)	Burning of the residual combustible material (°C)
CrZn(5)	50–155	155–245	>245
CrZn (15)	50–155	155–245	>245
CrZn (25)	50–150	150–245	>245

characteristic band at ~1384 cm^{-1}, corresponding to the antisymmetric stretching vibration. The "steamed bread" peak appearing at 3400–2200 cm^{-1} represented the O–H group. The band at 1720 cm^{-1} in the spectrum corresponds to the terminal free carboxyl groups of citric acid,[27] which means that there was citric acid remaining in the gel. The characteristic bands at ~1620 cm^{-1} represents the asymmetric stretching vibrations of the carboxyl ions (COO$^-$), while the band at 1550 cm^{-1} is attributed to the asymmetric stretches of (OCO) in the carboxylate species.[28–31]

Figure 3 shows the IR curves of the as-burnt powder. The characteristic bands of the carboxyl group and the ion in the IR spectrum appeared weak after combustion. The bands at ~560 and 620 cm^{-1} are associated with the vibration mode of O–Cr–O bond, confirming the formation of the Cr$_2$O$_3$ phase.[13] The characteristic band at 560 cm^{-1} shifted to 538 cm^{-1} for
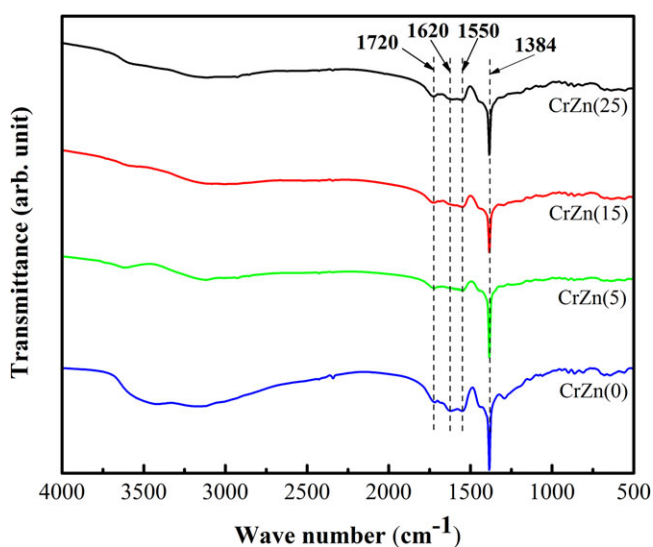
CrZn(15)-O and to 516 cm^{-1} for CrZn(25)-O, which may be due to the production of ZnCr$_2$O$_4$. Remarkably, the band at ~950 cm^{-1}, which is due to the stretching vibration of Cr–O–Cr in CrO$_4^{x-}$ (x = 2, 3, or 4), indicates that Cr with high valence (>3) was present.[32,33] The IR results show that the citrate ions and the nitrate ions fade away, and the Cr$_2$O$_3$ and chromite phases gradually appear during the combustion process.

Combining the TG-DTG and IR results, we can conclude that the clathrate compound turned into inorganic substances after the combustion process. The organic functional groups relevant to carboxylate species and ions took part in the oxidation–reduction reaction when the temperature was above 160°C. A large quantity of gas was released during the burning process. This left many tiny pores and resulted in a burnt sample with a high surface area. Finally, the chromium oxides to be used as catalyst precursors were obtained.

Characterization of catalysts

XRD of as-burnt powders and pre-fluorinated catalysts - Powder XRD studies were carried out on the burnt powders and the pre-fluorinated catalysts. No diffraction peaks related to citric acid or citrate were observed, implying that the combustion proceeded completely. In Figure 4(a), it can be seen that for the CrZn(0)-O and CrZn(5)-O samples, only diffraction peaks due to crystalline Cr$_2$O$_3$ are observed and no diffraction peaks of zinc or zinc oxide are found, which indicates that the

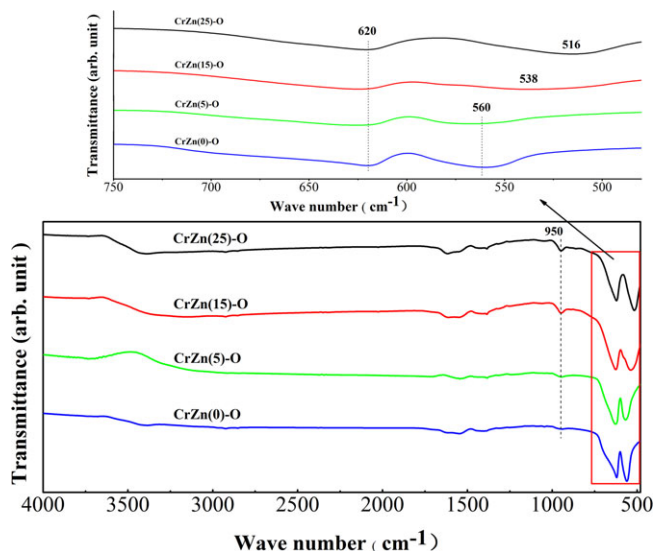Fig. 2. IR spectra of the dried gels.

Fig. 3. IR spectra of the as-burnt powders.

Zn species are well dispersed on the Cr_2O_3 surface as an amorphous or microcrystalline phase at low concentrations. There were both Cr_2O_3 and $ZnCr_2O_4$ phases in the CrZn(15)-O, and only $ZnCr_2O_4$ phase with a spinel structure was found in CrZn(25)-O. This indicates that crystalline $ZnCr_2O_4$ is easily formed for high Zn content. The diffraction peaks became relatively broad and weak with increased addition of Zn, which confirms the viewpoint[34] that an appropriate dopant causes a decrease in the crystallinity of the host lattice.
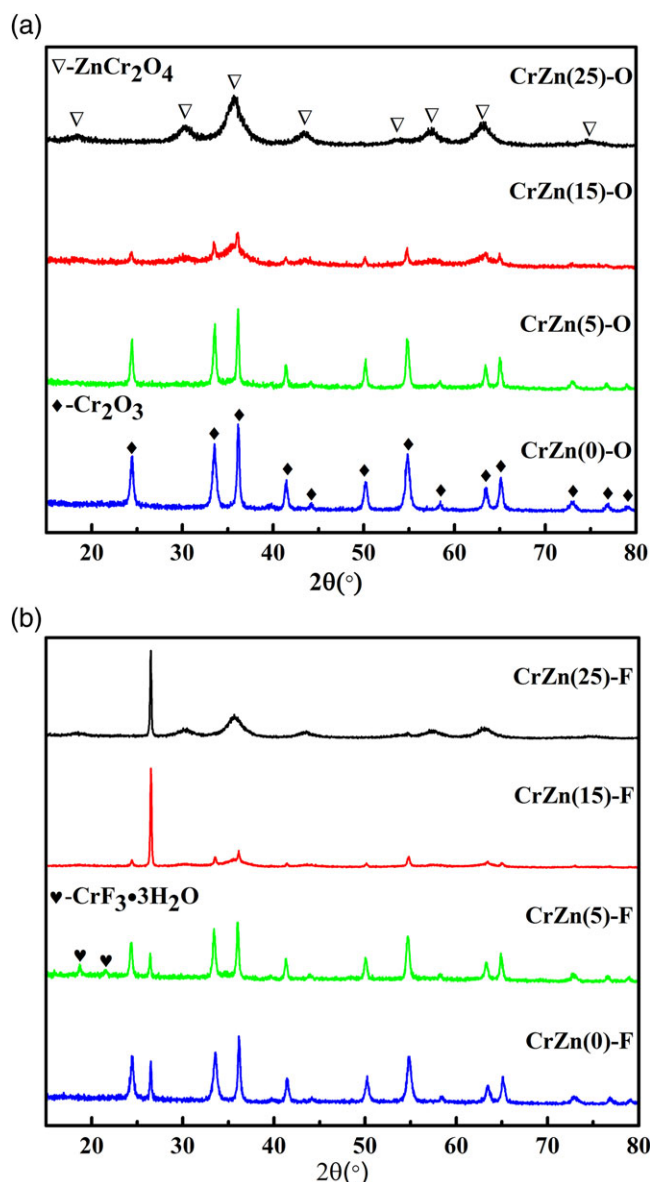

Fig. 4. XRD patterns of (a) burnt powders and (b) pre-fluorinated catalysts.

On comparing Figure 4(a) and (b), it can be seen that the diffraction peaks of the pre-fluorination catalysts and the as-burnt powder are almost identical, which suggests that the phase structure and composition remain stable during the fluorination. The crystalline phase $CrF_3·3H_2O$ was found in the CrZn(5)-F catalyst. It suggests that a small amount of Zn helps in reducing the crystallinity of Cr_2O_3 and forms unstable Cr species which are easily fluorinated. The diffraction peak at ~26.4° (2θ) is due to the graphite that was used in the mold. CrF_3 and $CrF_3·3H_2O$ are difficult to form because the free reaction enthalpy ($\bigtriangledown_R G = -68$ kJ/mol) for the formation of CrF_3 from the reaction of Cr_2O_3 with HF is only slightly less than zero.[35]

Morphology of as-burnt powders and pre-fluorinated catalysts SEM micrographs (Figure 5) show the pre-fluorinated catalyst as well as the as-burnt powder, which are composed of much smaller irregular-shaped particles. The particle size of the as-burnt powder was less than 100 nm, and it became ~200 nm after the pre-fluorination process. It can also be seen from the SEM images that all catalysts had a mesoporous structure and there were many micropores of irregular shape.

High-surface-area materials have unusual properties in heterogeneous catalysis, where the activity of the catalyst depends largely on its surface area.[36] The contact of the reactant gas with this high-surface catalyst would be enhanced, thus improving the reaction efficiency. The BET surface area, pore volume, pore diameter, and elemental analysis data of the fluorinated catalyst together with the data of the as-burnt powder are summarized in Table 2.

The surface area of the single-component oxide CrZn(0)-O is 124.8 m²/g. As the Zn content increases, the surface area of the CrZn(x)-O samples increases gradually, which suggests that the addition of Zn facilitates the high dispersion of the catalyst crystallites and, as a result, increases the BET surface area of the chromium oxide-based catalyst.[37,38] The surface area of the CrZn(x)-F catalysts first increases and then decreases upon further increasing the Zn, and CrZn(15)-F, with the largest surface areas of up to 139.4 m²/g, is the most accessible. The surface area was reduced by 41.75, 47.63, 12.59, and 23.94% for CrZn(0)-O, CrZn(5)-O, CrZn(15)-O, and CrZn(25)-O, respectively. The
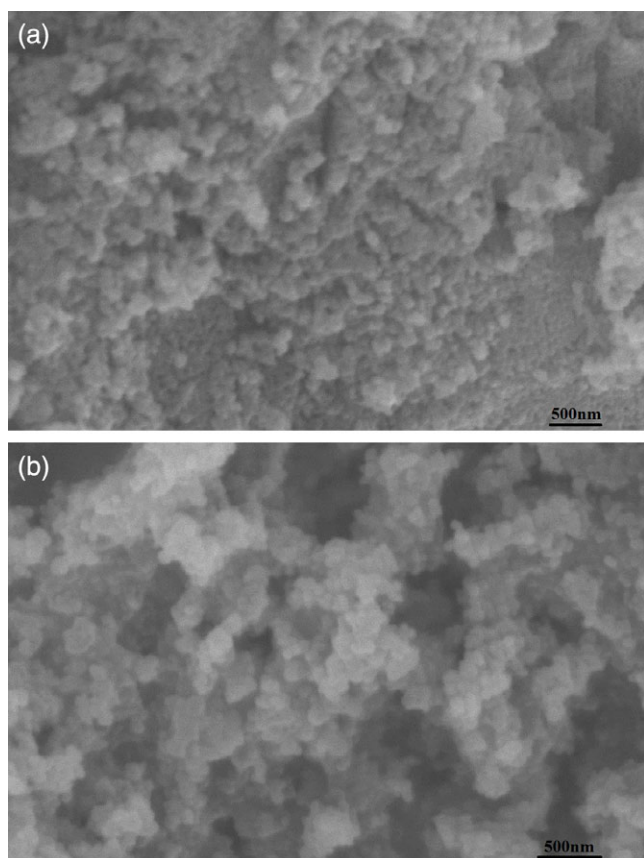
Fig. 5. SEM images of (a) CrZn(0)-O and (b) CrZn
(0)-F catalysts.

decrease in the specific surface area could correspond to the formation of fluorides or oxyfluorides.[39]

A pore size between 2 and 50 nm, called mesoporous, was observed for all of the samples. Figure 6 shows the N_2 sorption isotherms of the oxides and pre-fluorination catalysts. All samples displayed type IV isotherms, indicating that they are porous materials. Indeed, as can be seen in Table 2, the pre-fluorinated catalysts had a narrower pore size distribution than the catalyst precursors. For all CrZn(x)-O samples, the specific surface and pore volume decreased after the fluorination step. The pore volume was reduced by 28.6, 40, 15.4, and 14.3%.

Surface composition   XPS experiments were conducted to further investigate the Cr species on the catalysts surface. The Cr 2p XPS spectra of the pre-fluorination catalysts are shown in Figure 7. For all catalysts, the broad peak of Cr $2p_{3/2}$ could be de-convoluted into two peaks with binding energies (BEs) of 577.5 and 575.5 eV.

According to the literature,[37] the peak at 577.5 eV is attributed to the formation of CrO_xF_y species, which was deemed to be the active sites of fluorination.[40–42] Wagner[43] indicated that the Cr_2O_3 and $ZnCr_2O_4$ had the same Cr $2p_{3/2}$ BE, which is 575.5 eV in this study.

Table 3 lists the BEs of Cr $2p_{3/2}$ and CrO_xF_y surface contents of the CrZn(x)-F catalysts. The surface CrO_xF_y content was calculated by the peak area of CrO_xF_y divided by the total peak area of the Cr species. As can be seen in Table 3, with the addition of Zn, a shift toward a higher BE of the CrO_xF_y peak was observed, which could be attributed to the interaction of Zn with Cr. Additionally, the surface CrO_xF_y content in the CrZn(x)-F catalysts varied depending on the Zn addition. CrZn(15)-F had the highest content of surface CrO_xF_y species (71.2%), while the surface CrO_xF_y content of the CrZn(0)-F catalyst was the lowest (64.3%).

The Zn $2p_{3/2}$ XPS spectra of the pre-fluorination catalysts were analyzed as well. Figure 8 shows that after the treatment by HF, the zinc in the CrZn(5)-O sample was nearly completely fluorinated to ZnF_2. The presence of the mixed phase of $ZnCr_2O_4$ and ZnF_2 was also detected in the CrZn(15)-F catalyst. However, only the $ZnCr_2O_4$ phase was found in the CrZn(25)-F sample. According to Ref. 37 Zn at a relatively low concentration is more easily fluorinated. For a high Zn content, a simultaneous increase in the formation of aggregates of crystalline $ZnCr_2O_4$ makes it difficult to be fluorinated. Thus, when the amount of Zn on the catalyst surface is too low or too high, the formation of Cr_2O_3 or $ZnCr_2O_4$, which are difficult to fluorinate, is favored and the concentration of other species such as CrO_xF_y decreases.

Surface acidity   Lewis acids are commonly used as catalysts in fluorination reactions. It has been proposed that fluorination and disproportionation catalysts must possess Lewis acidity for their activities.[44] The FT-IR photoacoustic spectra of adsorbed pyridine were used for characterizing and identifying the type of acid sites in post-fluorinated catalysts. The results (Figure 9) confirm the presence of strong Lewis (L-Py) acid sites, as shown by the vibrational bands at 1454 and 1612 cm^{-1}. Brønsted acid sites (B-Py) at 1540 cm^{-1} were also found. Simultaneously, the band at ~1490 cm^{-1} can be assigned to both Lewis and Brønsted acid sites. Patil

Table 2. Textural properties of the oxides and pre-fluorination catalysts

	CrZn(x)-O			CrZn(x)-F		
Addition of Zn (mol%)	S_{BET}[a] (m²/g)	V[b] (cm³/g)	d_p[c] (Å)	S_{BET}[a] (m²/g)	V[b] (cm³/g)	d_p[c] (Å)
0	124.8	0.14	55	72.7	0.1	58
5	146.7	0.15	50	76.8	0.09	47
15	159.5	0.13	37	139.4	0.11	35
25	178.7	0.14	35	135.9	0.12	38

[a] BET surface area.
[b] BJH cumulative desorption pore volume.
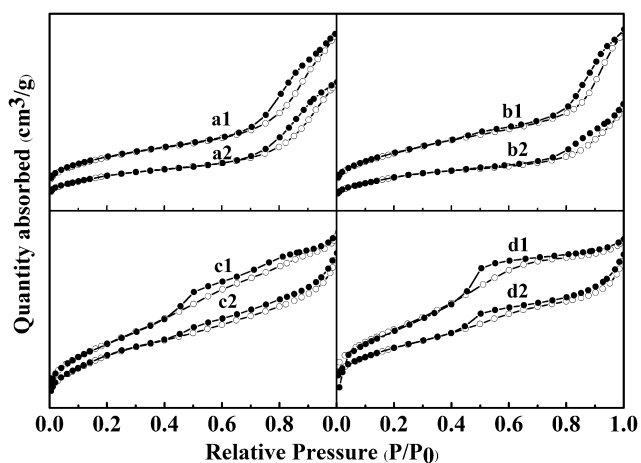[c] Mean pore diameter = $4V/S_{BET}$.

Fig. 6. Adsorption–desorption isotherms of the oxide samples and pre-fluorination catalysts: (a1) CrZn(0)-O, (a2) CrZn(0)-F; (b1) CrZn(5)-O, (b2) CrZn(5)-F; (c1) CrZn(15)-O, (c2) CrZn(15)-F; (d1) CrZn(25)-O, (d2) CrZn(25)-F.
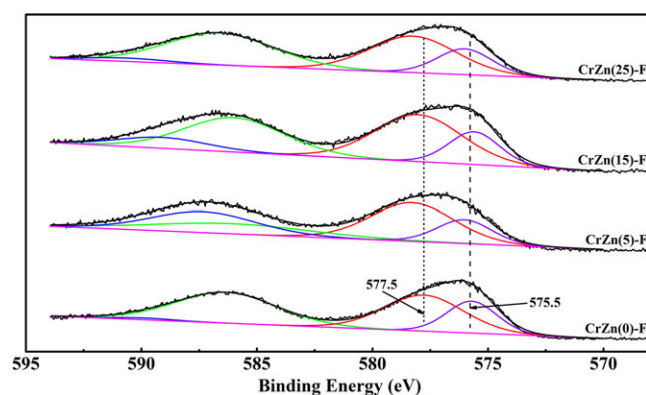

Fig. 7. XPS spectra of the Cr 2p level for CrZn(x)-F catalysts.

et al.[45] noted that the peak at ~1490 cm^{-1} is indicative of Brønsted sites only if its intensity exceeds that of the peak at ~1450 cm^{-1}. As seen from Figure 9, the number

of Lewis acid sites in CrZn(25)-F was the highest, and that of CrZn(0)-F was the lowest. However, the number of Brønsted acid sites first increased and then decreased upon increasing the Zn content, and the number of Brønsted acid sites in CrZn(15)-F catalyst was distinctly less than that in the other tested samples

A series of characterization experiments were carried out to further investigate the structure and properties of the catalysts prepared by the sol–gel auto-combustion method. It was found that the prepared catalysts had a much smaller particle size than those prepared by precipitation, which had micrometer-sized particles. For all CrZn(x)-F catalysts, the BET surface areas were higher than those of the Cr-based catalysts prepared conventionally by precipitation from aqueous media, exhibiting surface areas in the range 10–60 m²/g.[46] Chromium-based catalyst with 5 mol% zinc was prepared as well by the precipitation method in our laboratory. Post fluorination, the catalyst precursor was transformed into chromium fluoride, and only the CrF$_3$·3H$_2$O phase, which showed very low catalytic activity,[28] was found in the XRD. The content of CrO$_x$F$_y$ was ~66.4%, which is lower than that of the CrZn(5)-F catalyst prepared by sol–gel auto-combustion. The characterization results showed that the

Table 3. Binding energy of Cr 2p$_{3/2}$ and CrO$_x$F$_y$ surface content of CrZn(x)-F catalysts

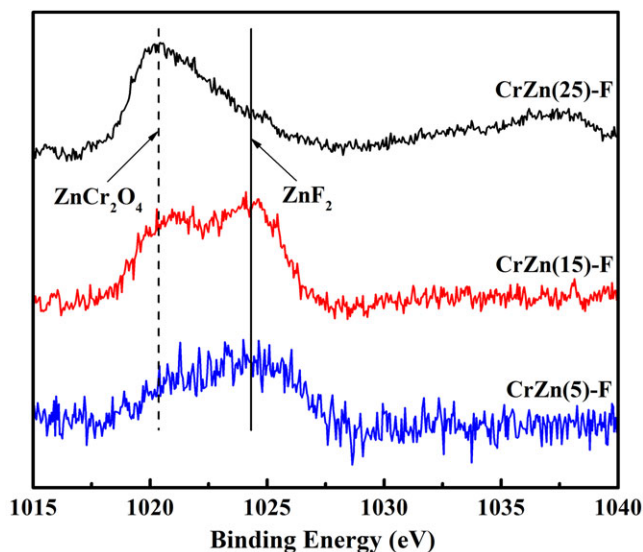|	Cr 2p$_{3/2}$/eV		Surface CrO$_x$F$_y$ content (%)
Catalysts	CrO$_x$F$_y$	Cr$_2$O$_3$/ ZnCr$_2$O$_4$	
CrZn(0)-F	577.5	575.5	64.3
CrZn(5)-F	578.3	575.9	70.8
CrZn(15)-F	578.1	575.6	71.2
CrZn(25)-F	578.2	575.9	68.5

Fig. 8. XPS spectra of the Zn $2p_{3/2}$ level for catalysts after treatment with HF.

catalysts prepared by the sol–gel auto-combustion method had smaller particle size, higher surface area, and higher content of surface active sites, all of which indicated that the catalyst prepared by this novel method should possess higher catalytic activity.

Performance of catalysts   To investigate the catalytic activity of the as-prepared CrZn(x)-F catalysts, the fluorination of 1,2-F6 to synthesize F7 was studied. As shown in Table 4, it is obvious that all catalysts show a

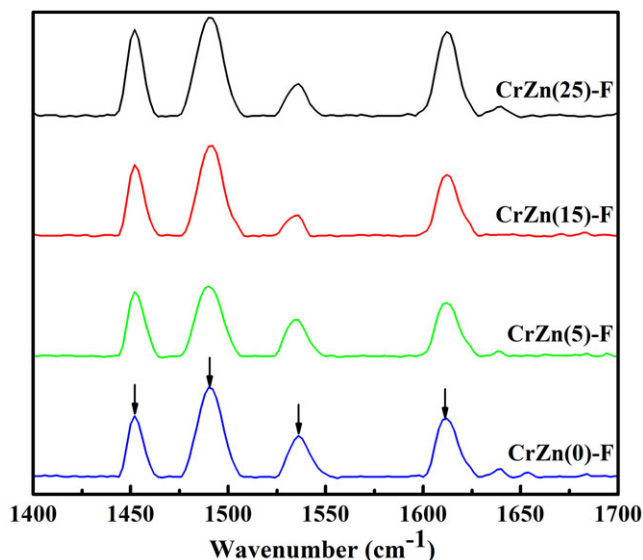Fig. 9. FTIR photoacoustic spectra of pyridine chemisorbed on CrZn(x)-F samples.

certain degree of catalytic activity for the fluorination of 1,2-F6. Especially, the conversion of 1,2-F6 reached 31.7% on the CrZn(15)-F catalyst at 430°C and its selectivity was 85.2%.

From Table 4, it can also be seen that the addition of Zn has a great influence on the catalytic activity. An increase of the activity for the synthesis of F7 was noticed when a small amount of zinc was added to the chromium-based catalyst; the conversion of 1,2-F6 and the selectivity to F7 reached maximum values at the Zn content of 15%. However, with further increase in the zinc content, the activity of CrZn(25)-F decreased obviously. On the other hand, the conversion of 1,2-F6 increased with increase in the reaction temperature for all the prepared catalysts. Yet, the selectivity of F7 declined with increase in the reaction temperature, and more of the by-product F8E was observed. When the reaction temperature reached 430°C, the selectivity of F7 was only 69.7% for CrZn(25)-F and the oligomers were detected.

Figure 10 shows the stability of the CrZn(x)-F catalysts at 400°C under reaction conditions. It can be seen that the conversion of 1,2-F6 slightly fluctuated in the initial period and then reached steady state after 3 h. The selectivity to F7 was below 80% during the first 3 h, but immediately increased to ~90% and stabilized for the CrZn(15)-F catalyst, which indicates that catalysts were quite stable during the reaction.

The unreacted 1,2-F6 was separated from the products by distillation and then recycled into the reactor system as raw materials. By this means, a method to produce F7 with a high yield was obtained. This demonstrates that the catalysts prepared by this novel auto-combustion method have a great value in industrial application.

An increase in the activity for the formation of F7 was noted when a small amount of zinc was added to the chromium-based catalyst. This is because the phase composition of the as-burnt powder CrZn(15)-O is complex and metastable, which is beneficial to the formation of the Cr active site CrO_xF_y (71.2% for CrZn(15)-F catalyst) after pre-fluorination. The BET surface area of the CrZn(15)-F catalyst is the largest (139.4 m^2/g). Besides, the number of Brønsted acid sites in CrZn(15)-F is less than that in the other prepared catalysts, which means that it has a higher relative number of Lewis acid sites. Thus the conversion of 1,2-F6 and the

Table 4. Effect of reaction temperature to 1,2-F6 conversions and F7 selectivity on CrZn(x)-F catalysts

| | Temperature (°C) | | | | | | | |
| | 350 | | 380 | | 400 | | 430 | |
Sample	C (%)	S (%)	C (%)	S (%)	C (%)	S (%)	C (%)	S (%)
CrZn(0)-F	3.7	90.7	8.6	87.4	16.9	85.5	21.7	79.8
CrZn(5)-F	4.6	92.5	11.6	88.7	20.7	86.7	27.2	82.3
CrZn(15)-F	7.1	94.3	19.6	89.2	24.9	90.3	31.7	85.2
CrZn(25)-F	2.9	85.6	9.8	79.3	16.3	76.5	21.9	69.7

Reaction conditions: HF/F6 molar ratio of 10 with contact time 12 s.
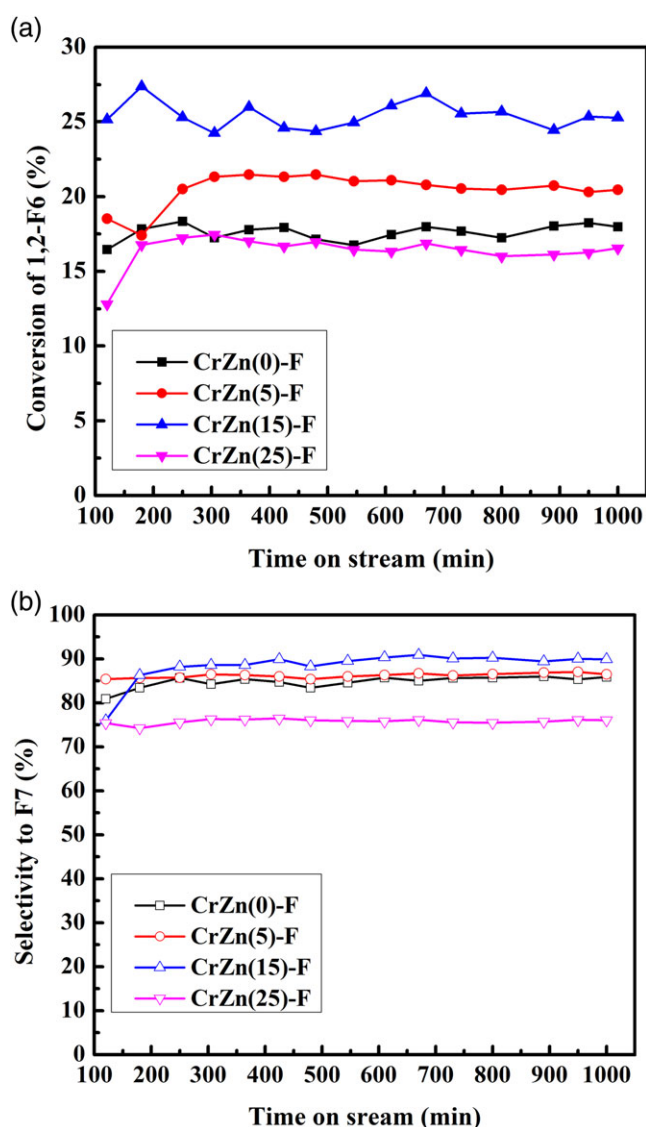C, conversion in %; S, selectivity in %.

(a)

(b)

Fig. 10. Relationship between the conversion of 1,2-F6 and the selectivity to F7 over CrZn(x)-F catalysts at 400°C and time on stream.

selectivity to F7 reach a maximum at the Zn content of 15%. However, upon further increasing the Zn content, the activity of CrZn(25)-F catalyst clearly decreased. This implies that when the amount of Zn on the catalyst surface is too high, the formation ZnCr$_2$O$_4$, which is difficult to fluorinate, is favored and the Cr active sites on CrO$_x$F$_y$ decreases. The number of Lewis acid sites in CrZn(25)-F was the largest. But olefin molecules could be easily adsorbed on the surface acid sites of the catalyst,[33,34] and the high surface acidity of the catalyst would result in rapid coke formation that blocks the active sites,[35] leading to a decrease in the specific rate of the reaction.

EXPERIMENTAL

Chemicals

Hexachlorocyclopentadiene was obtained from J&K Chemical Technology. Cr(NO$_3$)$_3$·9H$_2$O (>99%) and Zn(NO$_3$)$_2$·6H$_2$O (>99%) were obtained from Yunli Chemical Industry Co., Ltd., Shanxi, China. C$_6$H$_8$O$_7$·H$_2$O (>99.5%) and NH$_3$·H$_2$O (25–28%) were from Beijing Chemical Works Co., Ltd. AHF (>99%) was obtained from Sinochem Group.

Catalysts preparation

The nano-size chromium-based oxide was prepared by a unique combination of the chemical sol–gel process and the combustion process. First, stoichiometric amounts of chromic nitrate nonahydrate (Cr(NO$_3$)$_3$·9H$_2$O) and zinc nitrate hexahydrate (Zn(NO$_3$)$_2$·6H$_2$O) powders were dissolved in distilled water. The total molarity of the metal ions was 0.1 mol/L in solution (the mole rate of Cr^{3+}:Zn^{2+} is 100:0, 95:5, 85:15, 75:25 respectively). Then, a 0.1 mol/L citric acid solution was added dropwise to

the above solution till the molar ratio of metal ions/citrate ions reached 1:1.2. $NH_3 \cdot H_2O$ was added to the nitrate–citric solution, the pH value was adjusted to 3, and the mixture solution was prepared.

The mixture solution was thoroughly stirred for 12 h at 70°C, and water in the solution was vaporized gradually, when the solution become sticky. This sticky liquid was transferred into a drying oven and heated for 24 h at 80°C and 4 h at 120°C to obtain a dried gel. The dried gel was ignited and burned in a self-propagating combustion manner until it entirely changed to a loose powder. A schematic diagram of the preparation process is shown in Figure 11. Various samples with different mole rates of Cr^{3+}/Zn^{2+} was obtained by varying the relative proportions of $Cr(NO_3)_3 \cdot 9H_2O$ and $Zn(NO_3)_2 \cdot 6H_2O$. For mole rates of $Cr^{3+}:Zn^{2+}$ 100:0, 95:5, 85:15, and 75:25, the corresponding dried gels and burned dried gel were denoted as CrZn(0), CrZn(5), CrZn(15), CrZn(25), and CrZn(0)-O, CrZn(5)-O, CrZn(15)-O, and CrZn(25)-O, respectively.

Before the reaction, pre-fluorination was carried out to activate all catalyst precursors. A 5 g sample of the precursors was packed into the reactor. N_2 (150 mL/min) was passed through reactor at 250°C for 4 h to remove the water, which was followed by heating at 350°C for 4 h to decompose the residual organics in catalyst precursors. Then, a mixture of N_2 (100 mL/min) and AHF (50 mL/min) was passed through reactor at 250°C for 8 h. Then, the N_2 flow rate was decreased to 50 mL/min and AHF flow rate increased to 100 mL/min at 250°C. This mixture was fed into the reactor for 10 h. Subsequently, N_2 flow was stopped and the sample was heated at 350°C for 10 h in AHF at a flow rate of 150 mL/min. Finally, the pre-fluorination catalysts, denoted as CrZn(0)-F, CrZn(5)-F, CrZn(15)-F, and CrZn(25)-F, respectively, were formed.

Characterization of catalysts and gels

The characteristics and kinetics of the decomposition of the gel precursors were examined by a Perkin-Elmer TGA-2 instrument at the heating rate of 10°C/min under air and nitrogen. The sample weight was ~5 mg, and the gas flow rate was kept at 100 mL/min.

The IR spectra of the as-burnt powder were recorded on a Bomem DA 3.002 spectrometer from 400 to 4000 cm^{-1} by the KBr pellet method.

The structural characterization of the powders was performed by XRD using a Siemens D500 diffractometer with Cu Kα radiation in the 10–80° 2θ angle range at the scan rate of 0.3°/min. Phase composition and cell parameter were calculated by the Rietveld[47] method using the MID-JADE 6.5 software.

The specific surface areas were determined by the classical BET procedure using a Coulter SA 3100 apparatus.

The microstructure of the resulting ceramic was observed by SEM (Hitachi X-650).

XPS analyses were carried out using an M-probe apparatus (Surface Science Instruments). The accuracy of the reported BEs was estimated to be ±0.2 eV.

FT-IR photoacoustic pyridine adsorption spectroscopy was carried out according to the following procedure. A sample (80 mg) was pretreated at 150°C under a nitrogen flow of 35 mL/min for 15 min. Then, 60 mL pyridine was injected into the sample tube. The sample was flushed with nitrogen for 30 min to remove the physisorbed pyridine. Spectra of the sample were recorded at room temperature using an MTEC cell and FT-IR system 2000 (Perkin-Elmer).

The apparatus for the vapor-phase fluorination reaction was composed of a pump for transferring the liquid-phase reactant, HF, and N_2 mass flow controllers, and an electrically heated tubular Inconel reactor
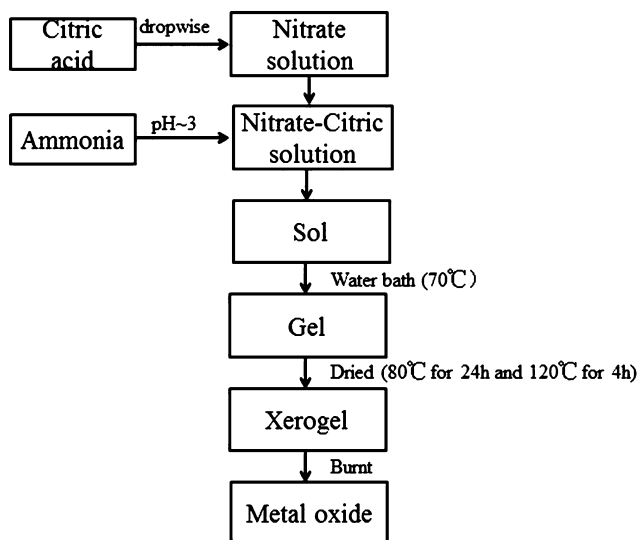

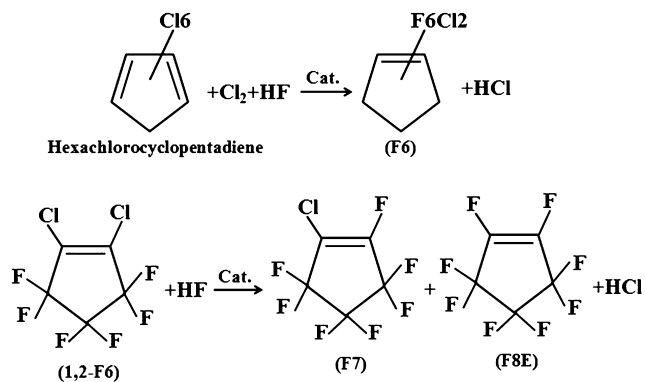Fig. 11. Diagram of the preparation of nano-sized CrZn(*x*)-O powders.

Fig. 12. Schematic diagram of the synthesis of 1-chloro-2,3,3,4,4,5,5-heptafluorocyclopentene (F7).

(14 mm in diameter and 300 mm in length) equipped with an inner Inconel tube for the insertion of type-K thermocouples with 1 mm diameter. The thermocouple enters the reactor through a Monel-type fitting and extends into the catalyst bed to measure the temperature changes at different positions along the reactor.

The synthesis of F7 from 1,2-F6

As shown in Figure 12, 1,2-F6 was prepared by the vapor-phase fluorination of hexachlorocyclopentadiene. The details are given in the patent application filed by our laboratory (CN201210254955.0).

Next, to prepare F7 and F8E, 1,2-F6(10 mL/min) and AHF (100 mL/min) were fed into a mixer at 150°C, and then passed through a reactor packed with 5 g of the catalyst at 350–430°C. The products were collected in an ice bath and washed by a dilute solution of KOH solution, and then the water was removed by anhydrous sodium sulfate and molecular sieves (4). The obtained products were analyzed by gas chromatography, GC-mass spectrometry, and ^{19}F NMR.

CONCLUSIONS

From the above experimental results, it is concluded that the dried nitrite–citrate gel can burn in a self-propagating combustion manner. Superfine metal oxide powders were directly synthesized via this sol–gel auto-combustion method. Then, the high-surface-area fluorination catalysts were obtained after the activation process, and particle size of the catalysts prepared by this method reached the nanoscale. The content of the catalytically active species and was high. The prepared catalysts showed commendable reaction efficiency for the fluorination of 1,2-F6, with the catalyst maintaining high activity and stability. Besides, the zinc content of the catalyst had a great influence on the structure and activity of the chromium-based catalyst, which illustrated that the addition of the promoter Zn should be moderate. It can therefore be concluded that the sol–gel auto-combustion method is very suitable for the preparation of high-surface-fluorination catalysts, and zinc is a very good doping agent for chromium-based catalysts used in the vapor-phase Cl/F exchange.

REFERENCES

1. M. J. Molina, F. S. Rowland, *Nature* **1974**, *249*, 810.
2. R. J. Salawitch, S. C. Wofsy, M. B. McElroy, *Planet. Space Sci.* **1988**, *36*, 213.
3. S. C. Wofsy, M. B. McElroyp, N. D. Sze, *Science* **1975**, *187*, 535.
4. H. Yu, E. M. Kennedy, A. Uddin, S. P. Sullivan, B. Z. Dlugogorski, *Int. J. Chem. Kinet.* **2005**, *37*, 134.
5. Y. Hu, Y. Xu, T. Wang, C. Wang, S. Li, *J. Anal. Appl. Pyrolysis* **2011**, *90*, 27.
6. T. J. Wallington, W. F. Schneider, D. R. Worsnop, O. J. Nielsen, J. Sehested, W. J. Debruyn, J. A. Shorter, *Environ. Sci. Technol.* **1994**, *28*, 320A.
7. A. McCulloch, *J. Fluorine Chem.* **1999**, *100*, 163.
8. X. M. Zhou, W. W. Chen, M. Y. Chao, G. X. Liao, *J. Fluorine Chem.* **2013**, *153*, 101.
9. S. Wuttke, S. M. Coman, J. Krohnert, F. C. Jentoft, E. Kemnitz, *Catal. Today* **2010**, *152*, 2.
10. H. D. Quan, Z. Li, Z. X. Zhao, H. E. Yang, J. Lu, *Appl. Catal. B: Environ.* **1996**, *8*, 209.
11. T. Yoshimura,Y. Homoto, Y. Yamada, T. Tsuda, T. Shibanuma, Process for producing pentafluoroethane and tetrafluorochloroethane U.S. Patent 6,011,185, **2000**.
12. B. Cheminal, E. Lacroix, A. Lants, Process for fluorination of perchloroethylene or of pentachloroethane U.S. Patent 5,932,776, **1999**.
13. P. Gibot, L. Vidal, *J. Eur. Ceram. Soc.* **2010**, *30*, 911.
14. J. L. Delattre, P. J. Chupas, C. P. Grey and A. M. Stacy, *J. Am. Chem. Soc.* **2001**, *123*, 5364.
15. S. Rudiger, U. Groß, E. Kemnitz, *J. Fluorine Chem.* **2007**, *128*, 353.
16. F. Zhang, D. Y. Zhao, *ACS Nano* **2009**, *3*, 159.
17. M. H. Cao, C. W. Hu, E. B. Wang, *J. Am. Chem. Soc.* **2003**, *125*, 11196.
18. U. Kurtan, R. Topkaya, A. Baykala and M. S. Toprak, *Ceram. Int.* **2013**, *39*, 6551.
19. K. H. Wu, T. H. Ting, M. C. Li and W. D. Ho, *J. Magn. Magn. Mater.* **2006**, *298*, 25.

20. D. Kovacheva, H. Gadjov, K. Petrov, S. Mandal, M. G. Lazarraga, L. Pascual, J. M. Amarilla, R. M. Rojas, P. Herrero, and J. M. Rojo, *J. Mater. Chem.* **2002**, *12*, 1184.

21. A. Saberi, F. Golestani-Fard, H. Sarpoolaky, M. Willert-Porada, T. Gerdes, R. Simon, *J. Alloys Compd.* **2008**, *462*, 142.

22. F. T. Li, Y. Liu, Z. M. Sun, R. H. Liu, C. G. Kou, Y. Zhao, D. S. Zhao, *Mater. Lett.* **2011**, *65*, 406.

23. R. Ianos, I. Lazau, C. Pacurariu, P. Barvinschi, *Mater. Res. Bull.* **2008**, *43*, 3408.

24. S. Habibzadeh, A. Kazemi-Beydokhti, A. A. Khodadadi, Y. Mortazavi, S. Omanovic, M. Shariat-Niassar, *Chem. Eng. J.* **2010**, *156*, 471.

25. K. H. Wu, C. H. Yu, Y. C. Chang and D. N. Horng, *J. Solid State Chem.* **2004**, *177*, 4119.

26. Z. X. Yue, J. Zhou, L. T. Li, H. G. Zhang and Z. L. Gui, *J. Magn. Magn. Mater.* **2000**, *208*, 55.

27. L. Shi, K. Tao, R. Q. Yang, F. Z. Meng, C. Xing and N. Tsubaki, *Appl. Catal. A: Gen.* **2011**, *401*, 46.

28. R. Q. Yang, Y. L. Fu, Y. Zhang, N. Tsubaki, *J. Catal.* **2004**, *228*, 23.

29. R. Srivastava, D. Srinivas, P. Ratnasamy, *J. Catal.* **2005**, *233*, 1.

30. A. Yee, S. J. Morrison, H. Idriss, *J. Catal.* **1999**, *186*, 279.

31. A. Yee, S. J. Morrison, H. Idriss, *J. Catal.* **2000**, *191*, 30.

32. R. B. Fahim, R. M. Gabr, M. J. Zaki and S. A. A. Mansour, *J. Colloid Interface Sci.* **1981**, *81*, 468.

33. P. Ratnasamyand, A. J. Leonard, *J. Phys. Chem.* **1972**, *76*, 1838.

34. B. Adamczyk, A. Hess, E. Kemnitz, *J. Mater. Chem.* **1996**, *6*, 1731.

35. B. Adamczyk, O. Boese, N. Weiher, S. L. M. Schroeder, E. Kemnits, *J. Fluorine Chem.* **2000**, *101*, 239.

36. G. Ertl, H. Knözinger, J. Weitkamp Eds., *Handbook of Heterogeneous Catalysis*, Wiley-VCH, Weinheim, **1997**.

37. A. Loustaunau, R. Fayolle-Romelaer, S. Celerier, *Catal. Lett.* **2010**, *138*, 215.

38. Y. X. Cheng, J. L. Fan, Z. Y. Xie, J. Q. Lu and M. F. Luo, *J. Fluorine Chem.* **2013**, *156*, 66.

39. C. Cochon, S. Celerier, A. Riviere, K. Vigier, J. D. Comparot, F. Metz and S. Brunet, *Catal. Commun.* **2010**, *12*, 151.

40. H. Lee, H. D. Jeong, Y. S. Chung, H. S. Lee, M. J. Chung, *J. Catal.* **1997**, *169*, 307.

41. E. F. Andrew, TaF.sub.5 and NbF.sub.5 as fluorination catalysts U.S. Patent 4,258,225, **1981**.

42. B. G. Lee, H. S. Kim, H. Kim, M. J. Chung, Method for concurrently producing 1,1,1,2-tetrafluoroethane and pentafluoroethane U.S. Patent 5,723,700, **1998**.

43. C. D. Wagner, In *Practical Surface Science*, Vol. *1*, D. Briggs, M. P. Seah Eds., Wiley, New York, **1993**.

44. M. Guisnet, J. Barrault, C. Bouchoule, D. Duprez and C. Montassler Eds., *Heterogeneous Catalysis and Fine Chemicals*, Elsevier, Amsterdam, **1988**, p. 257.

45. P. T. Patil, A. Dimitrov, H. Kirmse, W. Neumann and E. Kemnitz, *Appl. Catal. B: Environ.* **2008**, *78*, 80.

46. J. He, G. Q. Xie, J. Q. Lu, L. Qian, X. L. Zhang, P. Fang, Z. Y. Pu and M. F. Luo, *J. Catal.* **2008**, *253*, 1.

47. R. A. Young, *The Rietveld Method*, Oxford University Press, Oxford, **1993**.